JOURNAL OF GEOPHYSICAL RESEARCH, VOL. 93, NO. D11, PAGES 14,223–14,231, NOVEMBER 20, 1988

Radiative Properties of Desert Aerosols by Optical Ground-Based Measurements at Solar Wavelengths

D. TANRÉ, C. DEVAUX, M. HERMAN, AND R. SANTER

Laboratoire d'Optique Atmosphérique, Université des Sciences et Techniques de Lille Flandres Artois Villeneuve d'Ascq, France

J. Y. GAC

Institut Français de Recherche Scientifique pour le Développement de la Coopération, Dakar Hann, Sénégal

Radiation measurements were made during April and May 1986 at M'bour (16.9°W, 14.3°N), 80 km south of Dakar, Sénégal. The goal was to derive the optical properties of desert aerosols from ground-based measurements in order to validate satellite monitoring of these aerosols. We present here the results of a ground truth experiment. The measurements were performed during 15 nonconsecutive days in April and May 1986. Weather conditions varied during the experiment, as did the aerosol optical thickness (0.4–2 at 550 nm). The results are consistent with previous studies, notably Shettle's (1984) desert aerosol models; the aerosol characteristics were observed to depend upon the dust conditions, i.e., background or dust storm conditions.

1. INTRODUCTION

Atmospheric aerosols perturb the radiation budget of the Earth, and therefore they are justifiably considered as an important climatic factor [*Coakley and Cess*, 1985; *Potter and Cess*, 1984; *Rasool and Schneider*, 1971; *Tanré et al.*, 1984; World Climate Program (*WCP*), 1984]. Evidence for the desert aerosols is visible in the outbreaks of dust from West Africa, which are transported long distances through the atmosphere over the North Atlantic Ocean [*Joseph et al.*, 1973; *Joseph*, 1976].

In order to obtain global coverage and a good sampling of the aerosol characteristics at climatic scales, it is necessary to use satellite data. Thus we planned in 1986 an experiment for monitoring desert aerosols with different satellite sensors, the advanced very high resolution radiometer (AVHRR) on NOAA 9, Meteosat, and the Thematic Mapper on Landsat 5. A ground truth experiment was jointly conducted at M'bour (16.9°W, 14.32°N), Sénégal, in order to validate the results obtained from the satellite observations. We present here the ground results; the satellite data approach will be developed in a subsequent paper. The measurements performed (solar transmission, aureole, and sky radiance) are described in section 2. The data processing and the inversion method are examined in section 3. The aureole and solar transmission data classically are used to retrieve the aerosol size distribution. We use this data as input in a radiative code to calculate the sky radiance, which is checked against observations. These results are discussed in section 4.

2. PRESENTATION OF THE EXPERIMENT: INSTRUMENTATION

The ground station was based at M'bour in the Geophysic and Seismology center of the Institut Français de Recherche Scientifique pour le Développement de la Coopération (ORSTROM). This site was chosen because it is directly in the path of Saharan dust outbreaks. In fact, the major part of the dust is carried westward by the winds out over the North Atlantic and many investigations of this transport have been made [*Carlson and Prospero*, 1972; *D'Almeida*, 1986; *Morales*, 1986; *Prospero and Carlson*, 1981; *Schutz*, 1979]. These studies show that in winter months, the outbreaks emerge from Africa in the latitude belt 10°–20°N and are shifted to the north in summer. A more complete study in this area [*Gac and Carn*, 1986] confirms these results. The occurrence of outbreaks is much greater in winter than during summer; the concentrations are at a minimum in July and August and are at a maximum generally in March and April. Thus the experiment was planned for April and May 1986. M'bour was chosen in order to minimize the influence of local sources, Dakar being not really representative of Saharan dust because of the local anthropogenic component.

Table 1 sums up the performed ground measurements and their respective objectives. Three passive radiometric measurements were conducted: (1) extinction of the solar irradiance from 400 to 2200 nm; (2) scattered solar radiance in the aureole range at 850 nm; and (3) angular distribution of the sky radiance, in the solar incident plane, at 850 and 1650 nm.

1. Extinction measurements used two Sun photometers, which had the following main characteristics: (1) A portable radiometer (PR), whose the angular field of view was 3°, had five filters centered at about 450, 650, 850, 930, and 940 nm, with half-bandwidths ranging from 16 to 17 nm, except for the filter peaked at 930 nm, which had a 45-nm bandwidth. The two band-pass filters at 930 and 940 nm were used to derive the total atmospheric water vapor content from the differential absorption method. (2) The second radiometer (PIR, from "Proche Infrarouge" in French), whose the angular field of view was 3°, had seven filters centered at 450, 550, 650, 850, 1040, 1600, and 2200 nm. Thus we could determine the aerosol optical thickness over a wide range of wavelengths, as required for the aerosol size distribution retrieval.

2. Solar aureole measurements were performed at 850 nm, using a 1.5° angular field of view radiometer. Ten scattering

Paper number 88JD03348.
0148-0227/88/88JD-03348$05.00

TABLE 1. Summary of the Instrumentation

Instrument	Central Wavelength, nm	Measurements	Retrieved Physical Parameters
Portable radiometer	450, 650, 850, 930, 940	direct spectral solar radiance	optical depth water vapor content
Radiometer PIR	450, 550, 650, 850, 1040, 1650, 2200	direct spectral solar radiance	optical depth size distribution
Aureole meter	850	diffuse solar radiance	size distribution
Scanning radiometer	850, 1650	sky radiance	coherency of results

angles were sampled between 2° and 30° from the Sun direction.

3. Finally, the downward radiance was measured in the solar incident plane at two wavelengths, 850 nm and 1650 nm, with a 2° angular field of view. The angular scanning was sampled in steps by 3°. The radiometer was calibrated, and the accuracy on the radiance was estimated to be about 20% at 850 nm and 50% at 1650 nm.

These observations were performed during 15 nonconsecutive days in April and May 1986. A complete tabulation of the measurements is contained in Table 2. The transmission measurements were performed every day, but because of the discontinuous cloud cover, the other measurements were not always available. Table 2 shows that the whole set of measurements was available only on 4 days.

3. DATA PROCESSING

The inversion of the aerosol size distribution was performed in two independent ways: (1) from the optical thicknesses derived from the transmission measurements and (2) from the aerosol phase function in forward scattering directions derived from the aureole data.

First, the transmission measurements were corrected from the gaseous absorption and Rayleigh scattering effects, which provided the aerosol spectral optical thickness, $\tau_a(\lambda)$. Then, from $\tau_a(\lambda)$ the aerosol size distribution $n(r)$ was inverted. On the other hand, another estimate of $n(r)$ was obtained by inverting the aureole data, i.e., from the aerosol phase function, $p_a(\theta)$, in forward scattering directions. In fact, these two independent determinations of $n(r)$ prove to be somewhat complementary, because they are not efficient over the same particle radius ranges. Finally, given the retrieved aerosol model, the sky radiance was computed from a successive orders of scattering code [*Lenoble*, 1985], and the results were compared with the observations.

The correction for gaseous absorption in the transmission measurements was estimated as follows: The water vapor content was derived from the PR measurements at 930 and 940 nm. The method has been described by *Volz* [1974] among others. Given the characteristics of the two PR filters, Figure 1 shows how the transmission ratio t_g (940 nm)/t_g (930 nm) varies with the H_2O content for a given air mass m. Figure 1 corresponds to calculations based on the band model of Goody. From such curves, the H_2O content was derived from the measured transmission ratio with an accuracy of about 30%. As no direct estimates of the O_3 content were available, the *London et al.* [1976] mean value of 0.26 cm atm was assumed for O_3. Then, given the H_2O estimated content and the O_3 climatic content, the gaseous transmission was evaluated. When assuming for the O_3 and H_2O contents variations of 30% around their mean values (0.26 cm atm. and 3.5 g cm^{-2}, respectively), the variations obtained for the solar transmission proved to be equivalent to variations $\Delta\tau_a$ of the aerosol optical thickness no larger than 0.01 in the worst case (2200 nm). On the other hand, the molecular optical thickness τ_r was computed from the *McClatchey et al.* [1971] tropical atmosphere model. Finally, the observed transmissions were corrected from these estimated gaseous and molecular effects and provided the aerosol optical thickness $\tau_a(\lambda)$ in the seven bands of the PIR and in the three useful bands of the PR.

From the spectral dependence of $\tau_a(\lambda)$ derived in this way, the aerosol size distribution then was inverted, using the constrained linear inversion scheme developed by *King et al.* [1978]. The inversion was generally performed for an assumed refractive index of the aerosols $m = 1.55 - 0.005i$. Typically, $n(r)$ was retrieved in this way for r between 0.1 and 5 μm.

The aureole measurements allowed us to derive another independent estimate of the size distribution. This inversion is quite standard now (see, for example, *Thomalla and Quenzel* [1982]; *Trakhovsky and Shettle* [1985]; *Twitty* [1975]). Given the large optical thickness involved, the aureole measurements were first corrected from the multiple scattering contribution

TABLE 2. Summary of the Available Data

Date	Day	Instrument: Portable Radiometer	Radiometer PIR	Aureole Meter	Scanning Radiometer
April 28	118	X	X		
April 29	119		X		
April 30	120	X	X		
May 1	121	X	X		
May 2	122	X	X		
May 3	123	X	X		
May 4	124	X	X	X	X
May 5	125				
May 6	126		X		
May 7	127				
May 8	128	X	X	X	X
May 9	129	X	X	X	
May 10	130				
May 11	131	X	X	X	X
May 12	132	X	X	X	
May 13	133				
May 14	134				
May 15	135				
May 16	136		X		
May 17	137				
May 18	138				
May 19	139	X	X	X	X
May 20	140		X	X	X

Cross means measurement was made.

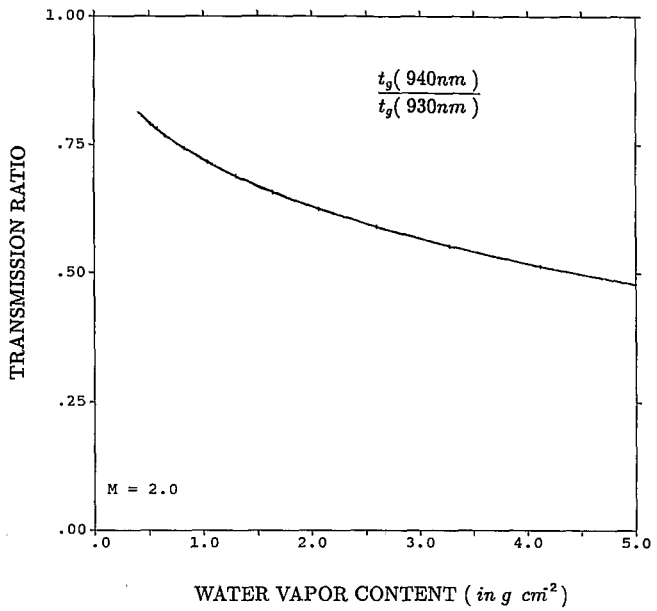

Fig. 1. Transmission ratio (narrow band over wideband filter) versus the H_2O content for an optical air mass $m = 2$.

by using the algorithm of *Weinman et al.* [1975]. Then, the data were inverted by using Chahine's inversion scheme [*Santer and Herman*, 1983]. This yielded the size distribution in the range 1–10 μm, so that we could check the two results in the common range of radius, typically 1–5 μm.

Finally, given the retrieved size distribution and an assumed refractive index $(1.55 - 0.005i)$, we computed from the Mie Theory the aerosol extinction coefficient, the single scattering albedo, and the phase function. These parameters, together with the aerosol optical thickness, were put in a successive orders of scattering code, and the downward radiance was calculated at 850 and 1650 nm. When compared with the measurements it provided a third independent check of the aerosol characterization.

4. Results and Discussion

4.1. *Water Vapor Content*

Figure 2 shows the time evolution of the measured U_{H_2O} content. The order of magnitude is in a good agreement with climatologic values [*Tuller*, 1968]: 2.5–4.5 g cm^{-2} according to the season and around 3 g cm^{-2} in April and May. As shown previously, H_2O requires only a small correction term in the measurements, so that the accuracy obtained in the U_{H_2O} estimates is sufficient.

4.2. *Aerosol Optical Thickness*

As the aerosol optical thickness was derived from two different instruments (Table 1), we first checked the consistency of the data by comparing the results in the three common spectral bands, i.e., 450, 650, and 850 nm. Figures 3*a* to 3*c* show, for these three channels, the aerosol optical thickness τ_a, derived from the PR measurements, versus the one derived from the PIR measurements. The measurements were not performed simultaneously by the two radiometers, but we selected, for the comparisons in Figure 3, measurements obtained within a maximum time delay of 2 min by the two apparatus. Given the accuracy on τ_a in the visible, about 5%, Figures 3*a* to 3*c* show that the results of the two instruments are in a good agreement. For the near- and middle-infrared channels, correlative measurements are not available. The errors are larger in this wavelength range, where the optical thickness is smaller and where the correction for the H_2O absorption can introduce residual errors. There, the estimated accuracy is probably no more than 10%, i.e., a factor 2 with respect to the visible accuracy.

The time variation of the aerosol optical thickness at 550 nm is shown in Figure 4. Each box represents a 1-hour interval, the x scale varies from 0700 to 1900 UT; and the y scale varies from $\tau_a = 0$ to $\tau_a = 2$. The dates are expressed as Julian days. Moreover, for each day the daily average and its variance σ_a have been reported. Figure 4 shows that the optical thickness varied widely from day to day, from 0.4 to 2. A major event, a dust storm, was observed on day 136 (May 16),

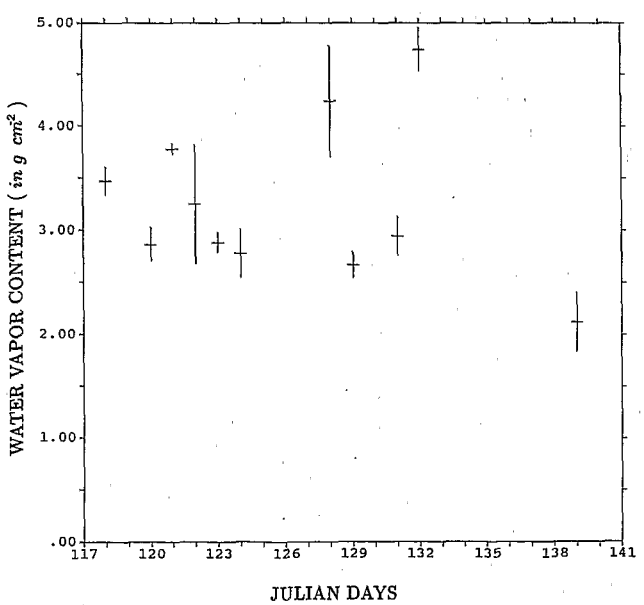

Fig. 2. Time evolution of the retrieved H_2O content. Error bars correspond to the diurnal variation.

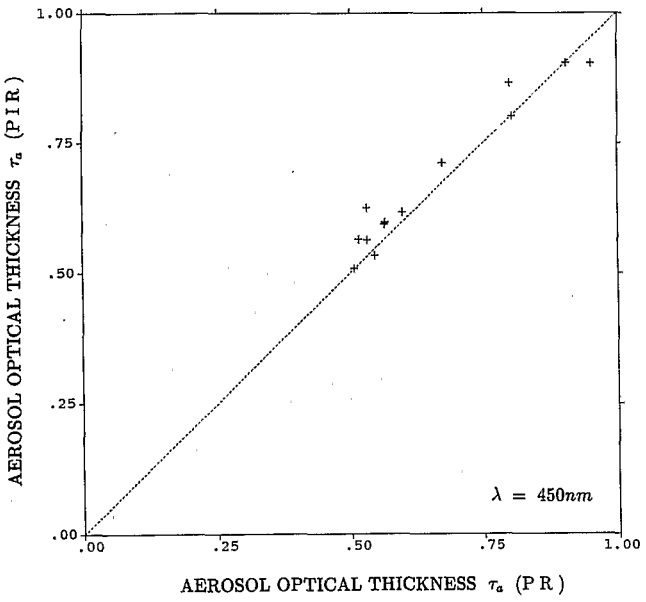

Fig. 3*a*. Aerosol optical thickness τ_a measured by the PR versus τ_a measured by the PIR at $\lambda = 450$ nm.

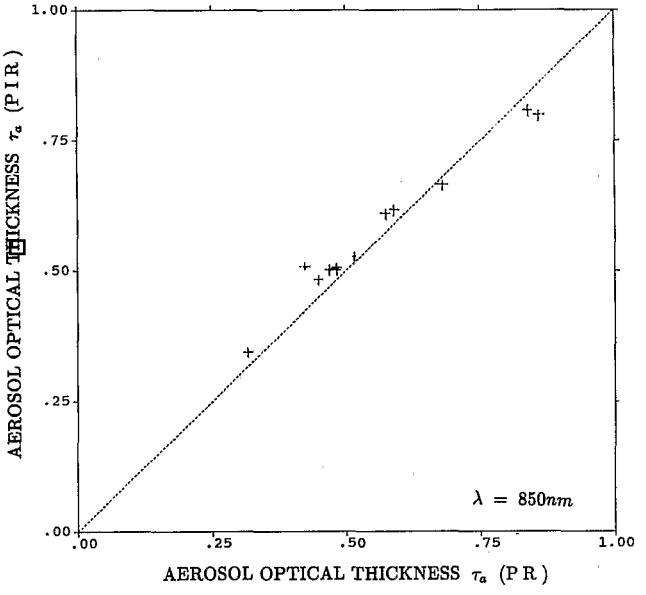

Fig. 3*c*. Same as Figure 3*a*, but for $\lambda = 850$ nm.

where τ_a reached the considerable value of 2. Unfortunately, the sky soon became cloudy on this day and only one measurement is available. The observations were started again 3 days later, and day 139 (May 19) was still affected by the event. The time evolution for this day was important. The optical thickness varied from 1.3 to 0.9, indicating the passage of the end of the dust plume. The next day (day 140), the optical thickness remained uniform and large ($\sim$0.85), corresponding to an important but uniform aerosol loading.

Figure 4 shows that the optical thickness was generally large. Even the minimum value ($\tau_a = 0.4$) observed on day 132 corresponded to a significant value. Thus the observations showed that a background desert component was persistent and might have a noticeable effect on the tropical solar energy budget.

From the spectral behavior of the aerosol optical thickness, one can infer some information regarding the size distribution by just looking at the variation of the Angström coefficient. For Saharan, dust the classical Angström turbidity coefficient α_a, defined by

$$\tau_a(\lambda) = C(\lambda)^{-\alpha_a} \tag{1}$$

is very small and can be even slightly negative over some wavelength interval [*Prospero et al.*, 1979; *Carlson and Caverly*, 1977]. Fluctuations of α_a reflect variations in the size spectrum.

Figure 5 shows a series of curves (in log-log scale) which illustrate the variations of the aerosol optical thickness as a function of the wavelength for 5 days. These days have been

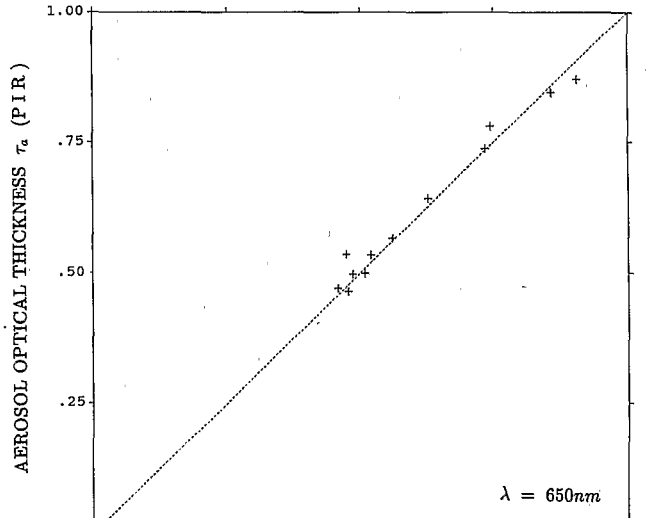

Fig. 3*b*. Same as Figure 3*a*, but for $\lambda = 650$ nm.

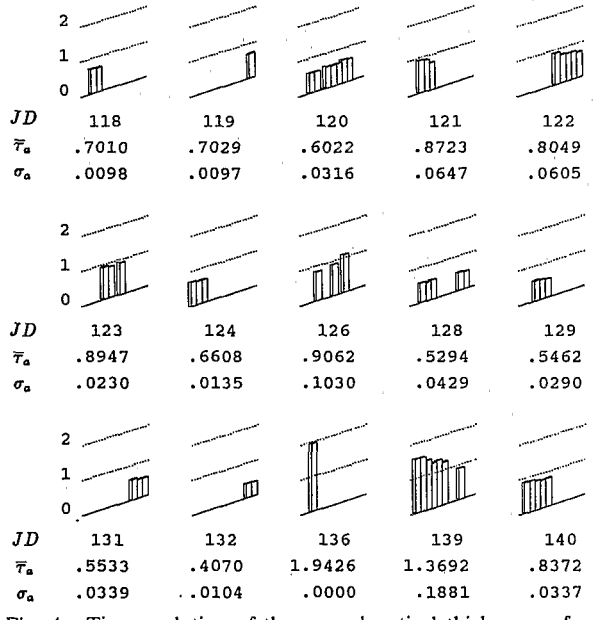

Fig. 4. Time evolution of the aerosol optical thickness τ_a for all the days of the experiment. Each box represents a 1-hour interval; the x scale varies between 0700 and 1900 UT, and the y scale varies between $\tau_a = 0$ and $\tau_a = 2$. The days are expressed as Julian days. Here $\bar{\tau}_a$ is the average aerosol optical thickness, and σ_a is the variance.

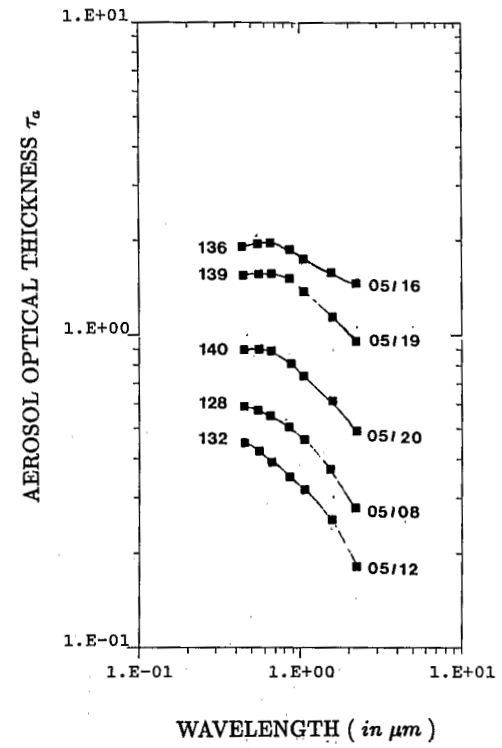

Fig. 5. Aerosol optical thickness versus the wavelength. Read 1.E + 01 as 1×10^1.

selected because they correspond to, (1) the clearest day (May 12); (2) the hazest day (May 16); (3) mean conditions (May 8); and (4) the days following the major event (days 139 and 140, on May 19 and 20). As noted, the results for May 16 correspond to only one measurement: they were retained because of their interesting behavior. Clearly, the spectral behavior of $\tau_a(\lambda)$ was correlated to the mean dustiness; the larger optical depths corresponded to the smaller mean coefficient α_a.

In the visible range (450–650 nm), α_a was slightly negative for very large turbidity (May 16 and 19). It became positive for mean dustiness conditions. In the infrared range the α_a behavior as a function of the turbidity was the same, but α_a here never became negative. For a Junge distribution, $n(r) = n_0 r^{-\nu}$, it is well known that $\alpha_a = \nu - 2$. Thus small values of α_a generally indicate high contents of large particles. It is evident that the observed size distribution did not compare with Junge distribution, but this crude analysis shows that the abundance of large particles was enhanced during the major event. This result agrees with the desert aerosol models developed by *Shettle* [1984], *Fouquart et al.* [1987], and *D'Almeida* [1987]. These authors discriminate the background desert aerosols from the desert dust storm aerosols, which differ significantly from their contents in larger particles.

4.3. *Evolution of Size Distribution*

Let us now consider the aerosol size distribution deduced from the spectral dependence of $\tau_a(\lambda)$ and from the angular dependence of the aerosol phase function $p_a(\theta)$, provided by the aureole measurements, respectively.

The optical thicknesses $\tau_a(\lambda)$ measured at seven wavelengths ranging from 450 to 2200 nm were inverted using the inversion scheme of King. The inversion was run for an assumed value of the refractive index $m = 1.55 - 0.005i$, according to *Patterson et al.* [1977]. As suggested by *Yamamoto and Tanaka* [1969], the exact range (r_{min}, r_{max}) over which the search for $n(r)$ was conducted was determined from preliminary trials. The results confirmed that whatever the case considered, the measurements did not allow one to retrieve $n(r)$ either for $r < 0.1$ μm (i.e., the nuclei mode) or for $r > 5$ μm (i.e., the coarse-particle mode).

On the other hand, from the sky radiances measured at

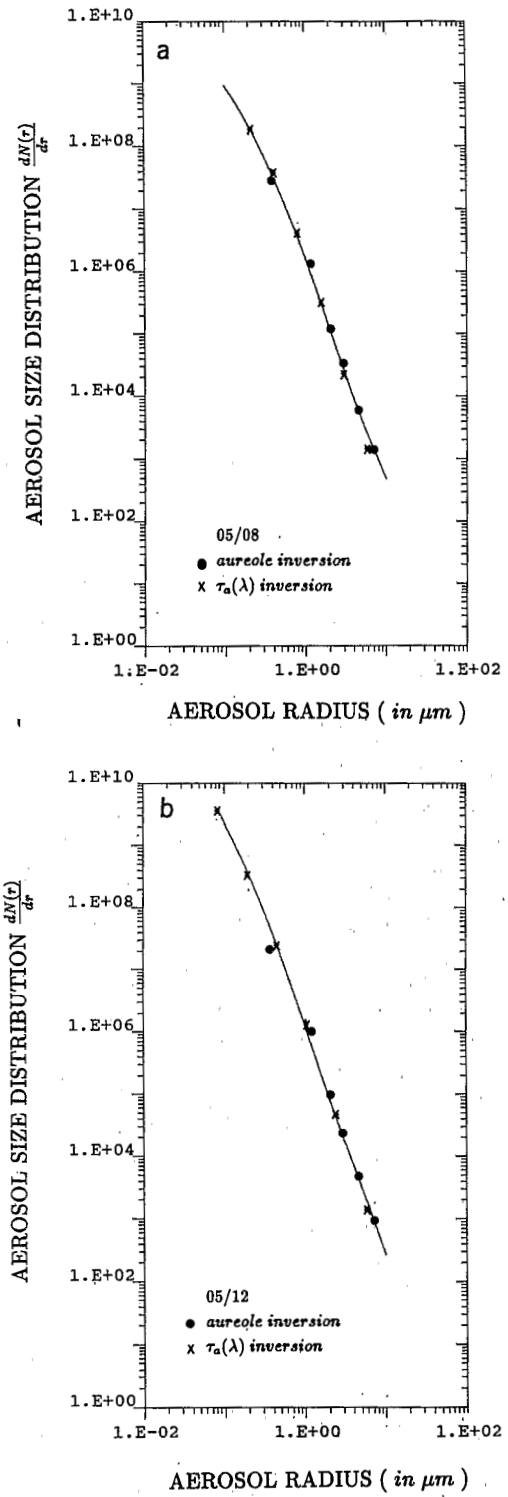

Fig. 6. Retrieved aerosol size distribution (per cubic centimeter) for (*a*) May 8, (*b*) May 12, and (*c*) May 19. The crosses correspond to the spectral optical thickness inversion; the solid circles correspond to the aureole inversion. Read 1.E + 10 as 1×10^{10}.

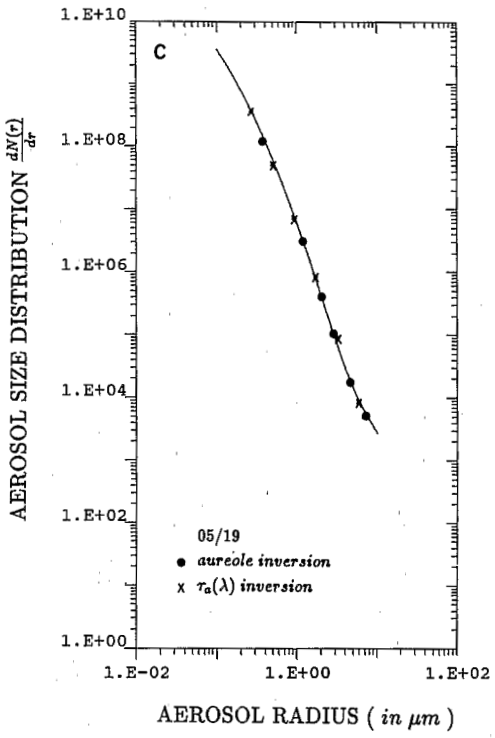

Fig. 6. (continued)

scattering angles ranging from 2° to 30°, another estimate of the size distribution was obtained by using the Chahine inversion scheme. The aureole data were first corrected for multiple scatterings, according to the method of *Weinman et al* [1975], and the corrected measurements allowed us to retrieve $n(r)$ for r ranging from about 1 to 10 μm. Note that the results are nearly insensitive to the assumed aerosol refractive index.

The two inversion schemes concern very different and independent observations. The spectral optical thickness provides

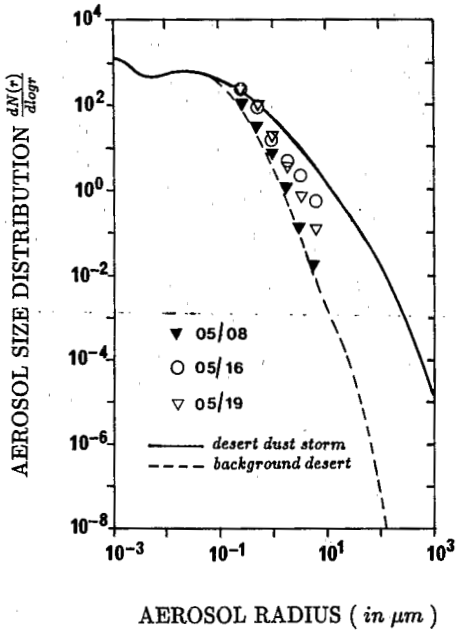

Fig. 7. Retrieved aerosol size distributions (per cubic centimeter) for May 8, May 16, and May 19, and the Shettle's aerosol model; dashed curve corresponds to the background desert model and the solid curve to the desert dust storm.

TABLE 3. Parameters of the Desert Aerosol Size Distribution

Date	r_1 (μm)	r_2 (μm)	σ_1	σ_2	N_2/N_1
May 12	0.03	0.30	0.5	0.5	3×10^{-4}
May 8	0.03	1.00	0.5	0.5	2×10^{-4}
May 19	0.03	3.00	0.5	0.5	7×10^{-5}

$n(r)$, in the range 0.1–5 μm, and the aureole, in the range 1–10 μm. By comparing the results over the range of radius 1–5 μm where both schemes are efficient, we may therefore check the consistency of the results.

As seen in Table 2, simultaneous transmission and aureole measurements were available for May 8 (mean concentration), May 12 (clearest day), and May 19 (very hazy day). We derived by the two inversion schemes the corresponding size distributions. The same index of refraction was used for the two inversions, and the retrieved size distributions were normalized in order to recover the optical thickness measured at $\lambda = 850$ nm. The results are shown in Figure 6. Solid circles represent the results of the aureole inversion, and the crosses represent the results of the optical thickness inversion. Clearly, the two results compare well and prove good consistency between the two kinds of observation.

In Figure 7 the results for May 8 and May 19 have been compared with size distributions reported by other authors [*Shettle*, 1984; *D'Almeida*, 1987], for background and dust storm conditions, respectively. We have reported also the results for May 16 (despite the lack of cross validation for this day, since only the PIR data are available) which represents the extreme dust loading during the experiment. Figure 7

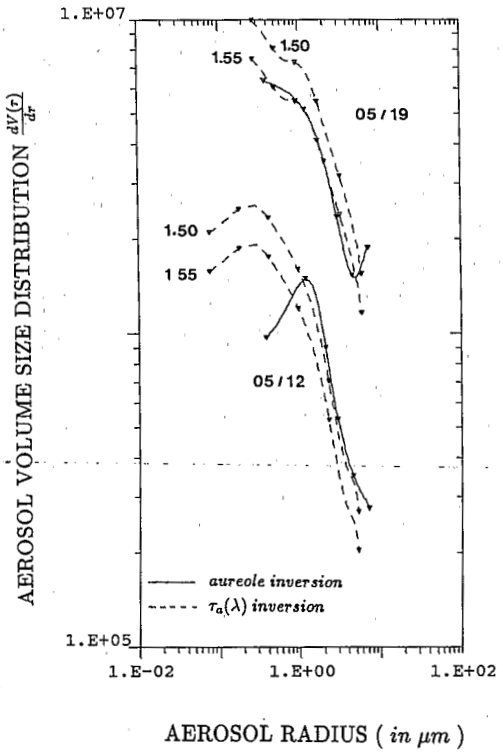

Fig. 8. Aerosol volume size distribution (cm^3/cm^3) for May 12 and May 19. The solid curve corresponds to aureole measurements; the dashed curve corresponds to optical thickness measurements. Two refractive indexes (1.50 and 1.55) have been considered. Read 1.E + 07 as 1×10^7.

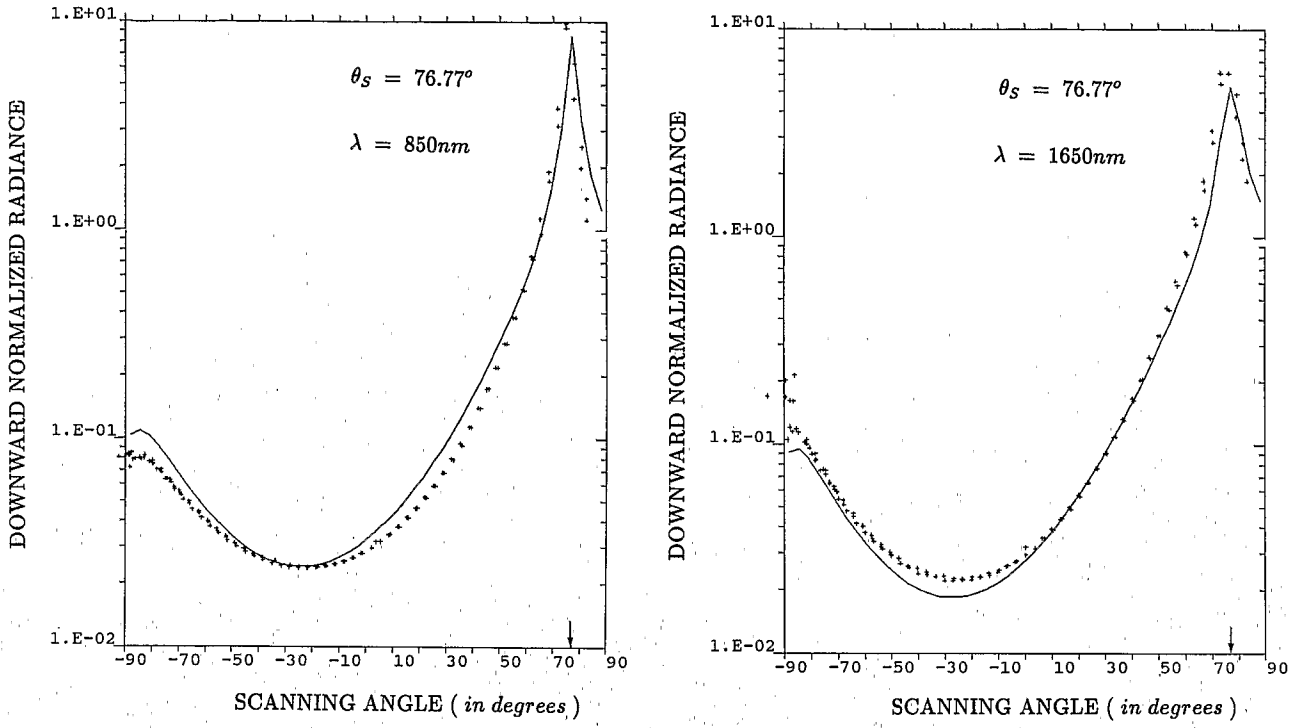

Fig. 9*a*. Diagram of the downward measured (plus signs) and computed (solid curve) radiances versus the scanning angle at 850 and 1650 nm for May 8. The Sun direction is shown by an arrow. Read 1.E + 01 as 1×10^1.

shows that our results are consistent with previous ones, and once more indicate that, as the dustiness increases, the size distribution exhibits an increasing amount of larger particles.

To make this tendency clearer, the observed size distributions were fitted by bimodal lognormal distributions,

$$\frac{dN(r)}{d\log r} = \sum_{i=1}^{2} \frac{N_i}{(2\pi)^{1/2}\log\sigma_i} \exp\left[\frac{(\log r - \log r_i)^2}{2(\log\sigma_i)^2}\right] \quad (2)$$

Table 3 gives the obtained parameters. To make the comparison, we fixed the same variance for the 3 days and for the two modes. The continuous curves, in Figures 6 and 7, correspond to these bimodal size distributions, which fit the results well. Table 3 shows that the second mode radius was shifted toward higher values for windblown dust conditions.

Moreover, the size distributions for the 2 extreme days were converted to volume distributions, so that variations in the

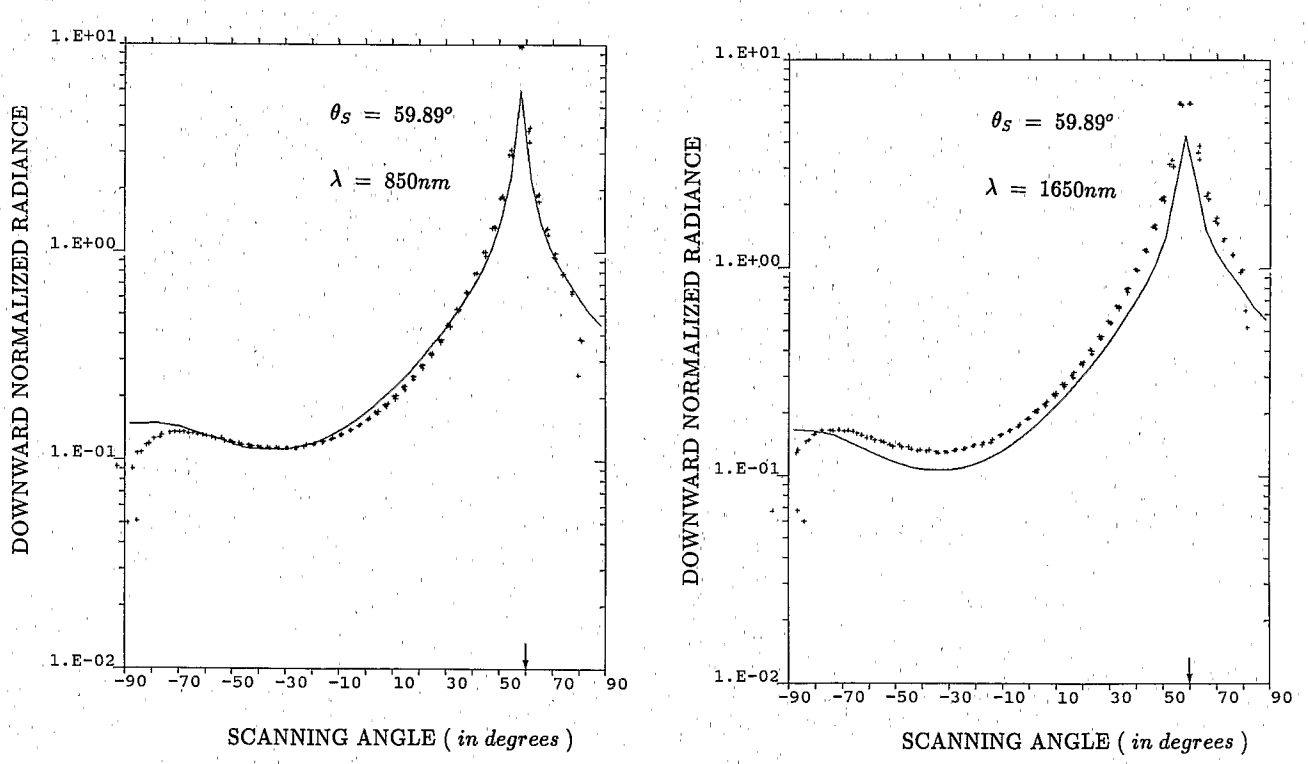

Fig. 9*b*. Same as Figure 9*a*, but for May 19.

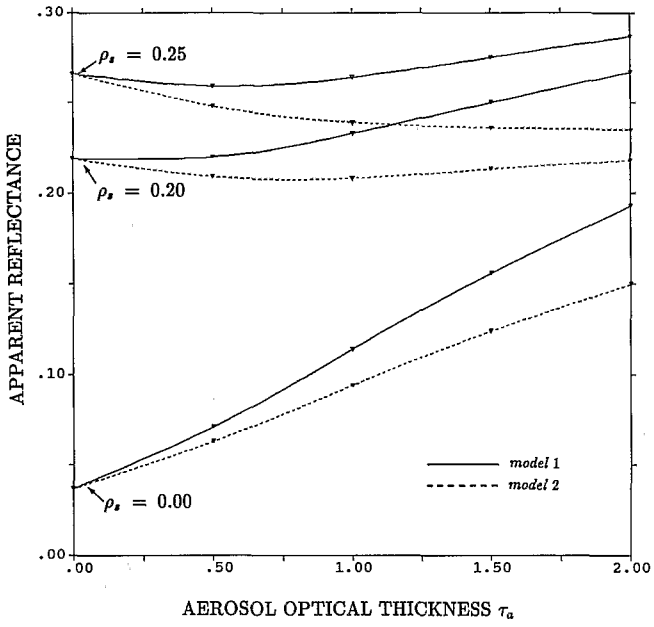

Fig. 10. Apparent reflectance at the top of the atmosphere for three values of surface reflectances (0.00, 0, 20, 0, 25), the two extreme aerosol models, and at $\lambda = 550$ nm. Geometrical conditions correspond to nadir observation and a Sun at 45° from the zenith.

large-particle range should be more evident (Figure 8). The enhancement of the large-particle abundance for the most turbid day is evident, especially in the aureole results, which are more confident for this range of radius. On the other hand, Figure 8 may give additional information on the aerosol refractive index. As noted previously, the aureole measurements, since they mainly correspond to diffracted light, are quite insensitive to the aerosol refractive index m. The same is not true for the aerosol optical thickness; given $n(r)$, $\tau_a(\lambda)$ partly depends on m. As shown by *Yamamoto and Tanaka* [1969], given the size distribution retrieved from $\tau_a(\lambda)$ by assuming some value, say m^*, for the aerosol refractive index, the size distribution corresponding to another value, m, may be scaled from

$$\frac{dN\{[(m^* - 1/m - 1)r]\}}{d \log r} = \left(\frac{m-1}{m^*-1}\right)^2 \frac{dN(r)}{d \log r} \qquad (3)$$

Then, starting from the size distribution retrieved from $\tau_a(\lambda)$ when assuming $m^* = 1.55 - 0.005i$, we scaled this size distribution according to (3), with different guesses for m, in order to fit the size distribution retrieved from the aureole data. We were able to make the two retrieved size distributions consistent in this way, in the range 1–5 μm, only when assuming $m = 1.50$ for May 12 and $m = 1.55$ for May 19. This seems to indicate that the composition of the aerosol is most similar to silicate material in dust storm conditions. This result is consistent with the common hypothesis of the dune material origin of the dust plume.

4.4. *Sky Radiance Reconstruction*

Given the retrieved aerosol size distribution, we calculated the aerosol single scattering albedo and phase function from the Mie theory. Then, given the measured optical thickness, we were able to compute the sky radiance by using the successive orders of scattering method. We took into account in the calculations a ground albedo estimated from the Thematic Mapper (TM) satellite data. The computations were performed, at 850 and 1650 nm, for the experimental geometrical conditions and with the measured aerosol optical thickness. The angular distribution of the downward sky radiance was computed in the principal plane and was compared with the measurements.

Figures 9*a* and 9*b* compare the results for May 8 and May 19. Given the large dynamic (10^2–10^3) of the involved signals and the calibration accuracy (about 20% at 850 nm, and no better than 50% at 1650 nm), the agreement between the computed and observed sky radiances is satisfactory and proves the consistency of the whole measurements. On the other hand, the good fit in Figures 9 suggests that the ground measurements allow us to make correct predictions of the satellite signal, whose the atmospheric reflectance is an important component. Therefore we used these results to examine crudely, according to our main goal, the possibility of remote measurements of the Saharan aerosol over the ocean and over the cloud.

In order to estimate the sensitivity of the method, the predicted satellite signal was calculated as a function of the aerosol optical thickness τ_a, for different values of the ground reflectance ρ_s($\rho_s = 0$, 0.20, and 0.25) and for the two extreme aerosol models reported in Table 3 (i.e., for $N_2/N_1 = 2 \times 10^{-4}$, say model 1, and for $N_2/N_1 = 7 \times 10^{-5}$, say model 2). Calculations were conducted for the observation geometry $\theta_v = 0°$, $\theta_s = 45°$, and for the observation wavelength $\lambda = 550$ nm. The results are shown in Figure 10.

For $\rho_s = 0$, which simulates crudely observations over the ocean, remote measurements of the aerosol are clearly feasible within a very large range of τ_a. For optical thicknesses smaller than 2 or 3, measurements should not be saturated, and variations of the aerosol characteristics within the expected range of models should lead to systematic errors in τ_a no larger than 10 or 15%.

On the contrary, for $\rho_s = 0.20$, which corresponds to the mean land reflectance of the experimental site, the problem is very ill conditioned. May be, Figure 10 is somewhat pessimistic; the single scattering albedo of our aerosol models, as derived from Mie theory for the assumed refractive index $m = 1.5 - 0.005i$, is $\omega_0 = 0.935$ for model 1 and $\omega_0 = 0.900$ for model 2, respectively. These rather small values, which explain the darkening effect of the aerosol layer for small optical thicknesses, may be questionable. Regardless of these particular effects, however, aerosol retrieval from reflectance measurements over highly reflecting lands certainly is a very difficult task; small inaccuracies in the estimate ρ_s of or small variations in the aerosol characteristics may clearly lead to very large errors in τ_a. Therefore, more elaborate methods have to be used to handle these types of calculations. Some possibility exists by considering, for example, contrast reductions linked to the aerosol blurring effect, as will be developed in a forthcoming paper.

5. CONCLUSIONS

Measurements of atmospheric transmission, solar aureole, and sky radiance were performed along the West African coast near Dakar, during April and May 1986, in order to characterize Saharan dust outbreaks. The main results were as follows:

1. The aerosol optical thickness varied widely from day to

day (0.4–2), and this thickness is large enough for satellite observation of such events.

2. A background desert component was persistent and might have an effect on the tropical solar energy budget.

3. Independent measurements were performed and gave consistent results by total different ways. These results confirmed the previous desert aerosols models.

4. Although the actual aerosol physical properties (refractive index and size distribution) were not perfectly retrieved, the results allowed us to calculate the radiative effects of a Saharan dust event with a good confidence.

Acknowledgments. This work was supported by the Centre National de la Recherche Scientifique (CNRS), under contract from ATP Aerosols Desertiques, and by le Centre National d'Etudes Spatiales (CNES). The authors wish to thank the Institut Français de Recherche Scientifique pour le Développement de la Coopération (ORSTOM) from Dakar and M'Bour and more particularly B. Dalmayrac and C. Villeneuve for their cooperation. They wish also to express their gratitude to the authorities of Senegal for their support.

REFERENCES

Carlson, T. N., and R. S. Caverly, Radiative characteristics of Saharan dust at solar wavelengths, *J. Geophys. Res.*, *87*, 3141–3152, 1977.

Carlson, T. N., and J. M. Prospero, The large-scale movement of Saharan air outbreaks over the Northern Equatorial Atlantic, *J. Appl. Meteorol.*, *11*, 283–297, 1972.

Coakley, J. A., and R. D. Cess, Response of the NCAR community climate model to the radiative forcing by the naturally occurring tropospheric aerosol, *J. Atmos. Sci.*, *42*, 1677–1692, 1985.

D'Almeida, G. A., A model for Saharan dust transport, *J. Clim. Appl. Meteorol.*, *25*, 903–916, 1986.

D'Almeida, G. A., On the variability of desert aerosol radiative characteristics, *J. Geophys. Res.*, *92*, 3017–3026, 1987.

Fouquart, Y., B. Bonnel, M. Chaoui Raquai, R. Santer, and A. Cerf, Observations of Saharan aerosols: Results of ECLATS field experiment, I, Optical properties and aerosols size distributions, *J. Clim. Appl. Meteorol.*, *26*, 28–37, 1987.

Gac, J. Y., and M. Carn, Importance des aérosols troposphériques de janvier 1984 à mars 1986 sur la presqu'île du Cap-Vert du Sénégal, *Bull. Veille Clim. Satell., Centre Meteorol. Sci. Lannion*, *12*, 52–55, 1986.

Joseph, J. H., The effect of a desert aerosol on a model of the general circulation, in *Proceedings of a Symposium on Radiation in the Atmosphere*, edited by H. J. Bolle, pp. 487–492, Science Press, Princeton, N. J., 1976.

Joseph, J. H., A. Manes, and D. Ashbel, Desert aerosols transported by Khamsinic depressions and their climatic effects, *J. Appl. Meteorol.*, *12*, 792–797, 1973.

King, M. D., D. M. Byrne, B. M. Herman, and J. A. Reagan, Aerosol size distributions obtained by inversion of spectral optical depth measurements, *J. Atmos. Sci.*, *35*, 2153–2167, 1978.

Lenoble, J., Radiative transfer in scattering and absorbing atmospheres: Standard computational procedures, 300 pp., A. Deepak, Hampton, Va., 1985.

London, J., R. D. Bojkov, S. Oltmans, and J. I. Kelley, Atlas of the global distribution of total ozone, July 1957—June 1967, *NCAR Tech. Note*, Natl. Cent. for Atmos. Res., Boulder, Colo., 1976.

McClatchey, R. A., R. W. Fenn, J. E. A. Selby, F. E. Volz, and J. S. Garing, Optical properties of the atmosphere, Environ. *Res. Pap. 354*, *AFCRL 71-0279*, Air Force Cambridge Res. Lab., Bedford, Mass., 1971.

Morales, C., The airborne transport of Saharan dust: A review, *Clim. Change*, *9*, 219–241, 1986.

Patterson, E. M., D. Gillette, and B. H. Stockton, Complex index of refraction between 300 and 700 nm for Saharan aerosols, *J. Geophys. Res.*, *82*, 3153–3160, 1977.

Potter, G. L., and R. D. Cess, Background tropospheric aerosols incorporation within a statistical dynamical climatic model, *J. Geophys. Res.*, *89*, 9521–9526, 1984.

Prospero, J. M., and T. N. Carlson, Saharan air outbreaks over the tropical North Atlantic, *Pure Appl. Geophys.*, *119*, 677–691, 1981.

Prospero, J. M., D. L. Savoie, T. N. Carlson, and R. T. Ness, Monitoring Saharan aerosol transport by means of atmospheric turbidity measurements, in *Saharan Dust: Mobilization, Transport, Deposition*, SCOPE *Rep. 14*, edited by C. Morales, John Wiley, New York, 1979.

Rasool, S. I., and S. H. Schneider, Atmospheric carbon dioxide and aerosols: Effects of large increases on global climate, *Science*, *173*, 138–141, 1971.

Santer, R. and M. Herman, Particle size distribution from forward scattered light using the Chahine inversion scheme, *Appl. Opt.*, *22*, 2294–2302, 1983.

Schutz, L., Saharan Dust transport over the north atlantic ocean—Model calculations and measurements, in *Sahara Dust: Mobilization, Transport, Deposition*, SCOPE *Rep. 14*, edited by C. Morales, John Wiley, New York, 1979.

Shettle, E. P., Optical and radiative properties of a desert aerosol model, *Proceedings of a Symposium on Radiation in the Atmosphere*, edited by G. Fiocco, pp. 74–77, A. Deepak, Hampton, Va., 1984.

Tanré, D., J. F. Geleyn, and J. Slingo, First results of the introduction of an advanced aerosol-radiation interaction in the ECMWF low resolution global model, in *Aerosol and Their Climatic Effects*, edited by H. E. Gerber and A. Deepak, pp. 133–177, A. Deepak, Hampton, Va., 1984.

Thomalla, E., and H. Quenzel, Information content of aerosol optical properties with respect to their size distribution, *Appl. Opt.*, *21*, 3170–3177, 1982.

Trakhovsky, E., and E. P. Shettle, Improved inversion procedure for the retrieval of aerosol size distributions using aureole measurements, *J. Opt. Soc. Am.*, *A2*, 2054–2060, 1985.

Tuller, S. E., World distribution of mean monthly and annual precipitable water, *Mon. Weather Rev.*, *96*, 785–797, 1968.

Twitty, J. T., The inversion of aureole measurements to derive aerosol size distribution, *J. Atmos. Sci.*, *32*, 584–591, 1975.

Volz, F. E., Economical multispectral sun photometer for measurements of aerosol extinction from 0.44 m to 1.6 m and precipitable water, *Appl. Opt.*, *13*, 1732–1733, 1974.

Weinman, J. A., J. T. Twitty, S. R. Browning, and B. M. Herman, Derivation of phase functions from multiply scattered sunlight transmitted through a hazy atmosphere, *J. Atmos. Sci.*, *32*, 577–584, 1975.

World Climate Program, Report of the experts meeting on aerosols and their climatic effects, *WCP 55*, edited by A. Deepak and H. E. Gerber, 107 pp., World Meteorol. Organ., Geneva Switzerland, 1984.

Yamamoto, G., and M. Tanaka, Determination of aerosol size distribution from spectral attenuation measurements, *Appl. Opt.*, *8*, 447–453, 1969.

C. Devaux, M. Herman, R. Santer, and D. Tanré, Laboratoire d'Optique Atmosphérique, Université des Sciences et Techniques de Lille Flandres Artois, 59655 Villeneuve d'Ascq Cedex, France.

J. Y. Gac, Institut Français de Recherche Scientifique pour le Développment de la Coopération, BP 1386, Dakar Hann, Sénégal.

(Received November 4, 1987;
revised July 27, 1988;
accepted July 29, 1988.)